IOPscience iopscience.iop.org

Home Search Collections Journals About Contact us My IOPscience

Interfacial dynamics and the static profile near a single wall in a model colloid–polymer mixture

This article has been downloaded from IOPscience. Please scroll down to see the full text article.

2003 J. Phys.: Condens. Matter 15 S245

(http://iopscience.iop.org/0953-8984/15/1/332)

View the table of contents for this issue, or go to the journal homepage for more

Download details:
IP Address: 171.66.16.97
The article was downloaded on 18/05/2010 at 19:24

Please note that terms and conditions apply.

INSTITUTE OF PHYSICS PUBLISHING JOURNAL OF PHYSICS: CONDENSED MATTER

J. Phys.: Condens. Matter **15** (2003) S245–S250 PII: S0953-8984(03)54704-X

Interfacial dynamics and the static profile near a single wall in a model colloid–polymer mixture

D G A L Aarts, J H van der Wiel and H N W Lekkerkerker

Van't Hoff Laboratory, Debye Research Institute, University of Utrecht, Padualaan 8, 3584 CH Utrecht, The Netherlands

E-mail: d.g.a.l.aarts@chem.uu.nl

Received 11 October 2002
Published 16 December 2002
Online at stacks.iop.org/JPhysCM/15/S245

Abstract

We report measurements on gas–liquid phase-separating colloid–polymer mixtures. A horizontally placed optical microscope with long-working-distance objectives enables us to see effects of gravity on phase separation kinetics and hence see the complete phase separation from beginning to end. Furthermore, the static profile near a single wall is analysed giving surface tensions in good agreement with scaling predictions as well as results from another experimental technique. The contact angle remains, however, intangible.

1. Introduction

Mixtures of colloids and non-adsorbing polymers display a rich phase behaviour, involving colloidal 'gas' (poor in colloid, rich in polymer), colloidal 'liquid' (rich in colloid, poor in polymer), and colloidal 'crystal' phases (ordered colloids, poor in polymer). These mixtures have proven to provide an excellent tool for studying fundamental processes such as equilibrium phase behaviour, phase transition kinetics, and metastable gel or glass states (for a recent comprehensive review, see [1]). By comparison, the interfacial tension between the coexisting phases has received little attention. The interfacial tension γ scales as the thermal energy (k_BT) divided by the square of the typical length scale d in the system, resulting in

$$\gamma \sim \frac{k_bT}{d^2}. \tag{1}$$

For colloid–polymer mixtures far from the critical point, d is of the order of the colloid diameter and the interfacial tension is thus at most a few μN m^{-1}. This ultralow interfacial tension has been measured [2–4]; this in turn invoked significant theoretical effort. Within the Asakura–Oosawa–Vrij model [5, 6] of colloid–polymer mixtures, in which polymers are treated as penetrable hard spheres, the interfacial tension and the wetting properties of such systems were calculated using density functional theory [7] and computer simulations [8].

 © 2003 IOP Publishing Ltd Printed in the UK

Both a Cahn-like wetting transition [9] and layering transitions upon approach to the critical point are predicted. The experimental verification of these predictions remains a challenge.

Here, we focus on the role of the interfacial tension in a gas–liquid phase-separating colloid–polymer mixture. The mixture will be introduced in section 2. Both the interfacial dynamics (section 3) and the resulting static interfacial profile near a single wall (section 4) are studied. We conclude and summarize our findings in section 5.

2. Experimental section

We used mixtures of spherical silica colloids and poly(dimethyl siloxane) polymers (PDMS, Janssen) in the solvent cyclohexane. This system was originally prepared by Verhaegh *et al* [10]. The colloids are commercially available Ludox spheres (Ludox AS 40% Dupont) coated with stearyl alcohol (1-octadecanol, Merck, zur synthesis) in order to provide steric stabilization [11]. The hydrodynamic radius of the particle was 13 nm with a polydispersity of 19% and the density was 1.60 g ml^{-1}. The radius of gyration of the polymers was determined as 14 nm, its molecular weight as 91 700 g mol^{-1} ($M_w/M_n = 1.9$), and the density as 0.976 g ml $^{-1}$. No signs were ever found that the polymer adsorbed on glass walls.

A Nikon Eclipse E400 POL optical microscope was placed horizontally and was equipped with standard 2× and 10× objectives and with Plan Fluor extra-long-working-distance (ELWD) 20× and 40× objectives with cover glass correction. Because of the use of the ELWD objectives, standard optical cuvettes (Hellma) could be used with a 1 mm optical path length. The use of such cuvettes enabled us to start measurements 5 s after homogenization and, moreover, increased the reproducibility. A Sony XC-8500-CE black-and-white video-camera module was attached to the microscope and was linked to a desktop computer. The maximum frame rate was 50 frames s^{-1} with a frame resolution of 72 DPI and a frame size of 768 × 576 pixels.

We will show pictures of samples with different colloid–polymer concentrations. All samples lie on the same dilution line (table 2) and display qualitatively the same behaviour although quantitatively at different times and with different sizes. We do not describe those differences in full detail, but rather show examples that illustrate the phenomena most clearly. All microscope images shown here have dimensions 706 × 528 μm and gravity always points downwards.

3. Interfacial dynamics

Once the interfaces between the demixing phase domains have become sharp the system enters the viscous hydrodynamic regime. The dynamics is then governed by an interplay between interfacial tension and viscous forces. From the quasi-static Stokes equation (with P the pressure, η the viscosity, and v the velocity),

$$\nabla P = \eta \nabla^2 v \tag{2}$$

we can derive the typical velocity. Using the fact that the capillary pressure P is proportional to γ/L, in which L is a typical length, and that the gradient terms scale as $1/L$, i.e.

$$P \sim \frac{\gamma}{L} \qquad \text{and} \qquad \nabla \sim \frac{1}{L}, \tag{3}$$

one can easily see that the typical capillary velocity v_c becomes

$$v_c \sim \frac{\gamma}{\eta}. \tag{4}$$

Table 1. Characteristic numbers for atomic/molecular and colloidal systems.

			Molecular	Colloidal
Interfacial tension	γ	(N m^{-1})	10^{-2}	10^{-6}
Viscosity	η	(Pa s)	10^{-3}	10^{-2}–10^{-1}
Density difference	$\Delta\rho$	(kg m^{-3})	10^{3}	10^{3}
Capillary length	l_c	(m)	10^{-3}	10^{-5}
Capillary velocity	v_c	(m s^{-1})	10^{1}	10^{-4}–10^{-5}
Scaling length	L_0	(m)	10^{-7}	10^{-1}–10^{1}
Scaling time	t_0	(s)	10^{-8}	10^{3}–10^{6}

In a colloidal system, $v_c \sim 10$–$100\ \mu$m s^{-1}, whereas in atomic/molecular systems, capillary velocities are of the order of 10 m s^{-1} (characteristic values are summarized in table 1). Inertia becomes important if the Reynolds number $Re = \rho v L/\eta$ becomes of order 1 and we can estimate when this happens by replacing the velocity v in Re by v_c [12–14]:

$$Re \approx \frac{\rho\gamma L}{\eta^2}. \tag{5}$$

Hence, inertia becomes important for lengths L larger than L_0 and at times t longer than $t_0 = L_0/v_c$:

$$L > L_0 = \frac{\eta^2}{\rho\gamma} \qquad \text{and} \qquad t > t_0 = \frac{\eta^3}{\rho\gamma^2}. \tag{6}$$

In table 1 we see that for colloidal systems inertia becomes important only at length scales and timescales much larger than in atomic/molecular systems and the viscous hydrodynamic regime is thus extended significantly with respect to the inertial hydrodynamic regime.

Looking at the dynamics of the colloid–polymer mixture described in section 2, we clearly see using light microscopy that density inhomogeneities have developed almost instantly (see figure 1(a) taken 5 s after homogenization), forming a clear spinodally decomposing mixture. After a short diffusive regime, interfaces coarsen and domains coalesce, driven by interfacial tension (figures 1(b)–(d)); the system is in the viscous hydrodynamic regime, first discussed by Siggia in the context of late-stage spinodal decomposition [15]. Up to figure 1, taken 20 s after homogenization, this behaviour looks very similar to lattice Boltzmann simulations for the viscous hydrodynamic regime [14], although those simulations were done for a 50–50% decomposing mixture. Experimentally, such a symmetric mixture is more difficult to obtain and here we have slightly more liquid than gas phase. The biggest difference stems, however, from the role gravity starts playing when structures are large enough, which is neglected in most computer studies on demixing systems. At a certain size (at $t \sim 23$ s) gravity starts pulling the heavy colloidal liquid and light colloidal gas phases apart, which results in hydrodynamic flow (figure 1(e)). After a certain time the system 'chooses' to increase the phase separation process by forming distinct vertical lanes (lane width $\sim 5\ \mu$m) of heavy phase moving down and light phase moving up (figure 1(f)). This looks very similar to the findings of recent calculations done by Löwen and co-workers [16], although these calculations were done for strongly interacting colloids driven apart by an external electric field. It is still unclear what exactly determines the beginning of lane formation and what ends it, although the local volume ratio between gas and liquid phase must play a role. It is furthermore not yet clear what sets the width of the lanes. After about 5 min hydrodynamic flow stops, because most of the material has phase separated. The final macroscopic interface between the two phases gradually emerges and becomes sharper, as can be seen in figure 2. Here, large liquid drops coalesce with their liquid bulk phase and the foam-like (Plateau borders are clearly visible) layer of these drops creams

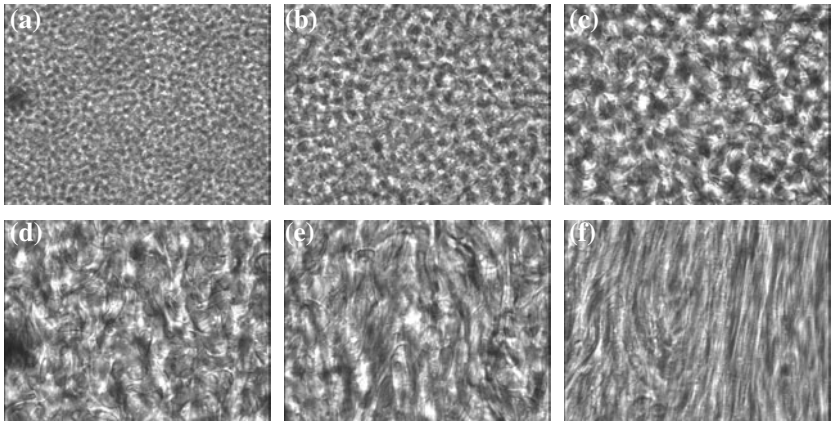

Figure 1. Optical microscopy pictures of a spinodally decomposing mixture taken (a) 5, (b) 10, (c) 15, (d) 20 s after homogenization. Coarsening and coalescence are clearly visible. After about (e) 23 s, hydrodynamic flow starts, resulting after (f) 32 s in lane formation. Sample IV.

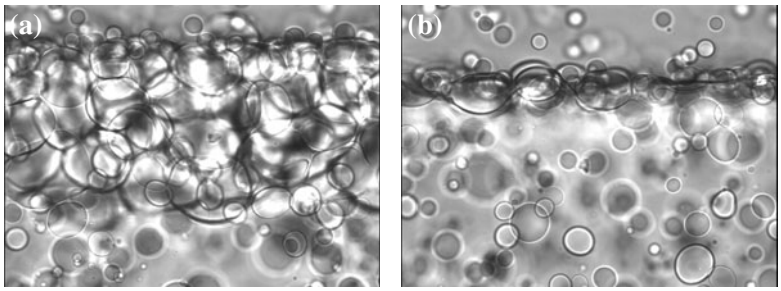

Figure 2. Optical microscopy pictures of interface formation taken (a) 6.30, (b) 6.50 min after homogenization. Large liquid drops lie on the macroscopic interface and coalesce with their bulk phase. In bulk gas and bulk liquid phase small droplets of the other phase are still present, which either rise or fall to the macroscopic interface. Sample II.

with a velocity of 20 μm s^{-1}, in agreement with the capillary velocity v_c. Furthermore, a droplet of size L coalesces with its bulk phase typically in time $t_c = L/v_c$ after the first break-up. After about 20 min the mixture has phase separated completely and a sharp interface between the two coexisting phases with a thickness $\sim\sigma_c$ [17] has formed.

4. Interfacial profile near a single wall

The interface between the two phases is very sharp and looks very flat to the naked eye near a wall (figure 3(a)). The capillary length is determined by the ratio between gravity and surface tension or

$$l_c = \sqrt{\frac{\gamma}{\Delta\rho\, g}} \tag{7}$$

and is of the order 10 μm (see table 1). It is however clearly visible with our microscopy set-up (see figure 3(b)). With the extra-long-working-distance objectives it is possible to focus into the sample and essentially obtain the static profile near a single wall. An analytic solution

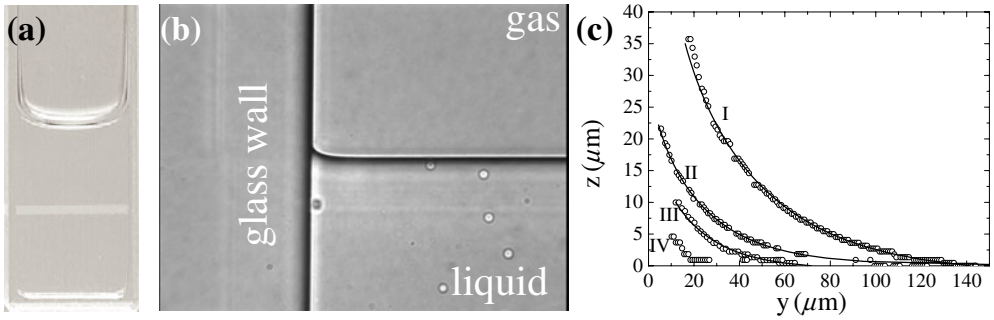

Figure 3. (a) A picture of our phase-separated colloid–polymer suspension. The cuvette is slightly tilted in order to show the interface better. (b) The interfacial profile near a flat wall. Clearly the liquid phase favours the glass wall. Sample II. (c) Measured profiles (open circles) for different samples (see table 2). Full curves are theoretical fits to (8).

Table 2. Volume fractions of colloid (ϕ_c) and polymer (ϕ_p relative to the overlap concentration), density differences $\Delta\rho$, experimental capillary lengths l_c, and interfacial tensions γ. All samples lie on the same dilution line.

Sample	ϕ_c	ϕ_p	$\Delta\rho$ (kg m^{-3})	l_c (μm)	γ (μN m^{-1})
I	0.254	1.94	320	32.9	3.38
II	0.217	1.66	256	26.5	1.76
III	0.208	1.59	233	16.0	0.58
IV	0.197	1.50	197	—	—

to the Young–Laplace equation (linking capillary pressure with curvature and surface tension) has been derived for the flat-wall case and is [18]

$$\frac{y}{l_c} = \left[\operatorname{arccosh}\left(\frac{2l_c}{z}\right) - \operatorname{arccosh}\left(\frac{2l_c}{h}\right) + \left(4 - \frac{h^2}{l_c^2}\right)^{1/2} - \left(4 - \frac{z^2}{l_c^2}\right)^{1/2}\right]. \quad (8)$$

This equation describes the distance y to the wall as a function of the height z above the flat interface. The maximum height for $y = 0$ is the capillary rise h. It can be shown mathematically that the capillary length l_c sets the shape of the profile, i.e. it is a self-similar profile which scales on l_c. This means that one only has to measure part of the profile to obtain l_c. If one knows the exact distance to the vertical wall, then it is possible to extrapolate the profile to where it hits the wall and thus obtain the capillary rise h. The contact angle θ with which the profile hits the wall can then be deduced from [18]

$$h^2 = 2l_c^2(1 - \sin\theta). \quad (9)$$

From figure 3(b) the profile between gas and liquid near the wall is clearly visible. The exact position of the glass wall is, however, difficult to obtain. The capillary length can still uniquely be determined by fixing h to some finite value and adding a constant to the rhs of (8) and thus treating the exact position of the wall as a fit parameter. With l_c as the only other fit parameter, the measured profile is very well described by (8) (full curves in figure 3(c)). We are now able to obtain γ since we know both l_c from the fit and $\Delta\rho$ from the phase diagram constructed [17]. Table 2 shows several values of the interfacial tension and the density difference upon approach to the critical point. The values of γ obtained here are in agreement with previous measurements using the spinning drop technique [3]. The contact angle depends very sensitively on the exact position of the wall and can change drastically close to the wall

(for example, 30° in only 2 μm for sample II). Hence, it remains intangible for now and we cannot yet say whether the interfacial profile is that of partial or complete wetting and whether there is a wetting transition upon approach to the critical point as predicted by Cahn [9].

5. Conclusions

Clearly, the ultralow interfacial tension leads to slow interfacial dynamics (figures 1(a)–(d)), which can be resolved by light microscopy. In principle, this allows detailed comparison with late-stage spinodal decomposition theories and simulations. Gravity, however, leads to hydrodynamic flow and this can ultimately lead to lane formation (figures 1(e) and (f)). The relatively slow collapse of the foam-like liquid layer on top of the macroscopic interface (figure 2) is another phenomenon worth studying.

The static interfacial profile near a single wall is uniquely defined by the capillary length, as it should be, and the resulting interfacial tensions are in agreement with previous measurements using a different technique. We cannot yet deduce the contact angle from this profile and precise measurements of the contact angle thus remain experimentally challenging.

Acknowledgments

The authors would like to thank Willem Kegel, Roel Dullens, Martijn Oversteegen, and Gert Aarts for useful discussions. This work was supported by the Stichting voor Fundamenteel Onderzoek der Materie (Foundation for Fundamental Research on Matter), which is part of the Nederlandse Organisatie voor Wetenschappelijk Onderzoek (Netherlands Organization for Advancement of Research).

References

[1] Poon W C K 2002 *J. Phys.: Condens. Matter* **14** R859
[2] Vliegenthart G A and Lekkerkerker H N W 1997 *Prog. Colloid Polym. Sci.* **105** 27
[3] de Hoog E H A and Lekkerkerker H N W 1999 *J. Phys. Chem.* B **103** 5274
[4] Chen B H, Payandeh B and Robert M 2000 *Phys. Rev.* E **62** 2369
[5] Asakura S and Oosawa F 1958 *J. Polym. Sci.* **33** 183
[6] Vrij A 1976 *Pure Appl. Chem.* **48** 471
[7] Brader J M, Evans R, Schmidt M and Löwen H 2002 *J. Phys.: Condens. Matter* **14** L1
[8] Dijkstra M and van Roij R 2002 *Phys. Rev. Lett.* at press
[9] Cahn J W 1977 *J. Chem. Phys.* **66** 3667
[10] Verhaegh N A M, van Duijneveldt J S, Dhont J K G and Lekkerkerker H N W 1996 *Physica* A **230** 409
[11] Helden A K and Vrij A 1980 *J. Colloid Interface Sci.* **76** 418
[12] Bray A J 2000 Coarsening dynamics of nonequilibrium phase transitions *Soft and Fragile Matter: Nonequilibrium Dynamics, Metastability and Flow* ed M E Cates and M R Evans (Edinburgh: SUSSP Publications)
[13] Lister J R and Stone H A 1998 *Phys. Fluids* **10** 2758
[14] Pagonabarraga I, Desplat J C, Wagner A J and Cates M E 2001 *New J. Phys.* **3** 91
[15] Siggia E D 1979 *Phys. Rev.* A **20** 595
[16] Dzubiella J, Hoffmann G P and Löwen H 2002 *Phys. Rev.* E **65** 021402
[17] de Hoog E H A, Lekkerkerker H N W, Schulz J and Findenegg G H 1999 *J. Phys. Chem.* B **103** 10657
[18] Batchelor G K 1967 *An Introduction to Fluid Dynamics* (Cambridge: Cambridge University Press)